Performance of the Hall D Tagger Microscope as a Function of Rate

R.T. Jones
University of Connecticut, Storrs, CT

December 30, 2010

Abstract

The Hall D tagger microscope is responsible for determining the energy and indirectly, the polarization, of the photon beam for the GlueX experiment. A detailed design for the tagger microscope has been completed and prototyped by the University of Connecticut group, based on scintillating fiber detectors and a silicon photomultiplier (SiPM) readout. An earlier Monte Carlo study indicated that this design would be capable of running at the maximum design luminosity of 10^8 γ/s on target in the primary polarized peak, with a time resolution better than 200 ps, a detection efficiency of 95% and a tagging ratio close to 70%. This conclusion has recently come into question, as more information has come to light about the long-term performance of SiPM devices, in particular the increase in dark rate that has been observed as a result of their exposure to neutron radiation. This paper presents results from a detailed Monte Carlo study of the performance of a single tagger microscope channel, in terms of detection efficiency and time resolution, as a function of both beam intensity and and detector dark rate. This study improves upon the earlier work in that it takes into explicit account published performance parameters of specific SiPM devices, whose values in the prior study were in some cases only guessed. The conclusion of the study is that the CPTA 2 mm SiPM from Photonique that was used in the prototype is not capable of reaching the stated performance goals, but that the 3 mm Hamamatsu device does satisfy these requirements at the full operating beam intensity for Gluex, in the presence of a dark rate as high as 10^{10} Hz, which is a factor 2500 higher than the dark rate of the pristine device. Extrapolating existing measurements of dark rate as a function of neutron dose, this corresponds to a lifetime limit of 550,000 hours (63 years) of continuous running in the unshielded Hall D tagger microscope at the nominal beam intensity of 10^8 γ/s. This remarkable robustness of the readout, in the presence of elevated dark rate, is a consequence of the combination of large photon yield in the microscope, and the fast pixel recovery time of the Hamamatsu SiPM.

1 Introduction

The Hall D tagging spectrometer detector package consists of two subsystems: a coarse-grained array of 190 counters spanning the range 3.0 - 11.7 GeV photon energy with 30 MeV bins, and a fine-grained "microscope" covering the range 8.3 - 9.1 GeV photon energy with 8 MeV bins. The microscope is focused on this specific photon energy range because significant beam polarization exists only in a restricted energy region around the primary coherent peak in the window 8.4 - 9.0 GeV. GlueX has been designed to be able to run at collimated beam intensities up to 10^8/s within this energy window, which requires that the microscope be capable of running at a total tagged rate of 2.4×10^8/s integrated over the same energy range. To handle this rate, the microscope is segmented into 100 non-overlapping energy channels and covers the somewhat larger energy region 8.3 - 9.1 GeV to allow for small variations in the coherent peak position while running. This leads to a modest requirement on the microscope readout electronics that it run efficiently and with good time resolution at rates up to 4 MHz per channel. Table 1 lists the design goals for the tagger microscope, which enable near-optimum performance of the tagger for GlueX physics, subject to the constraints of a coherent bremsstrahlung source.

1.1 optimization of microscope design

One property in Table 1 that requires explanation is the *post-collimator tagging ratio*. Also sometimes known as "tagging efficiency", the *tagging ratio* is the rate of tagged photons in a particular energy bin that reach the target, divided by the total counting rate in the corresponding tagger channel. Ordinarily one would like this ratio to be close to unity, but there is a trade-off between polarization and tagging efficiency in the Hall D photon beam design that comes from the choice of the collimation angle; photons that strike the collimator do not contribute to the numerator in the tagging ratio, but their corresponding electrons do get counted in the denominator. The particular choice made for Gluex results in a near-optimum polarization of 40% at 9 GeV, but at a tagging ratio that is around 50%. This poor tagging ratio can be significantly improved by collimating the post-bremsstrahlung electrons to within a thin band around the horizontal scattering plane, so that those with large vertical projections of their momentum vector are not detected in the tagging counters. The photons produced by these electrons have a similarly large vertical momentum component, and so are blocked by the collimator. Making the tagger blind to these electrons improves the tagging ratio without impacting the rate of tagged photons that reach the target, hence improving the performance of the tagger by decreasing the rate of accidental tags.

The only reliable way to achieve this within the existing spectrometer geometry, without introducing more background from scattering than is eliminated by collimation, is to vertically segment

Table 1: Design specifications for the Hall D tagger microscope. These goals enable near-optimum performance of the tagger for GlueX physics, within the constraints of a coherent bremsstrahlung source designed for 40% polarization at 9 GeV produced using 12 GeV electrons.

parameter	value	unit
tagging rate per energy bin (peak)	4.0	MHz
tagged electron detection efficiency	95	%
tagged electron time resolution	200	ps
post-collimator tagging ratio	70	%

the tagging detector array, and count only the vertical segment that subtends the momentum region corresponding to the photon collimator. Monte Carlo studies have shown that a 2 mm stripe across the focal plane contains nearly all of the photons that pass through the collimator, while eliminating about half of those that do not pass. The improved value of 70% in Table 1 reflects this capability. The microscope focal plane is constructed as a two-dimensional array of 2×2 mm^2 scintillator cells, whose 100 columns constitute the tagged energy bins and whose 5 rows are used both for tagging (central row, 70% of count rate) and active monitoring of the out-of-plane scattering rates (2 rows above and 2 below), for a total of 500 readout channels.

1.2 overview of readout design

The readout of light pulses from the individual square scintillating fibers that make up the detector array is done using SiPM's. Clear acrylic fibers glued to the exit end of the 2 cm scintillating fibers carry the light from the spectrometer focal plane to a coupler which aligns the ends of the light guides with the positions of the SiPM's mounted on a circuit board. Also integrated together in the same detector-mounted electronics package are the preamplifiers and summing circuits for the readout signals, and the programmable bias voltage control for the SiPM's. The decoupling of the readout from the detectors with clear-fiber light guides allows the electronics to be located some distance from the detectors in a shielded area. In the present design, the electronics are located within the same housing less than 50 cm from the detectors.

1.3 lifetime from radiation damage

A critical concern with the design outlined above has arisen within the past year, as new data have come to light regarding the sensitivity of SiPM devices to ionizing radiation, particularly protons and neutrons [3]. In a comprehensive study by Y. Qiang [1], SiPM devices from CPTA (Photonique), Sensl, and Hamamatsu were exposed to varying calibrated doses of neutron radiation up to 150 rem. The results of the study are more or less uniform, that gain and quantum efficiency are not affected after exposure to neutrons, but that dark current increases in a linear fashion with neutron dose, with a slope that is large enough to produce measurable effects after only a few hours of operation in the Hall D tagger area.

A simulation study recently published by A. Somov [2] reports neutron dose estimates in the position of the tagger microscope of 180 mrem/h at nominal beam intensity of 10^8 γ/s. This dose rate can be combined with the results from Ref. [1] to estimate what the dark rate would be after 10 years of operation of the Hall D beam. The CPTA 2×2 mm^2 device from Photonique starts out with a dark rate of 10 MHz. After 40 rem of neutrons at an operating temperature of 24 C, the persistent dark rate has increased by a factor 5 to 50 MHz, corresponding to 200 hours of tagger operation at full intensity. Extrapolating forward with a constant slope, the dark rate is 7×10^9 Hz after 30,000 hours of operation. Periodic annealing of the electronics boards at 60 C might reduce that rate estimate by 30%. The Hamamatsu S10931 device starts off at a somewhat lower dark rate of 4 MHz and scales up to about 3×10^9Hz after 10 years. The following sections present the results of a detailed study investigating the effects of increased dark rate on the detector performance, specifically in terms of time resolution and detection efficiency.

2 Simulation Model

The model presented here is comparable to that reported in Ref. [5], and a simplified version of the more complex model reported in Ref. [10]. A SiPM consists of many identical photodiodes arranged in a square grid array on the surface of a silicon wafer. The cells of the grid are separated from each other by v-shaped trenches that cut down through the active layer of the device, and serve to electrically and optically isolate the pixels from their neighbors. Each pixel acts as an independent avalanche photodiode (APD) operating in Geiger mode. Quenching of the Geiger pulse is provided by a resistor R_q which operates in conjunction with the internal capacitance C_1 of the diode structure to determine the charge q_1 released by an individual avalanche event and the time constant τ_1 for recharging the junction to its full reverse-bias operating potential V_b which is set a small amount ΔV above the breakdown threshold potential V_0.

$$q_1 = C_1 \, \Delta V \tag{1}$$

$$\tau_1 = R_q \, C_1 \tag{2}$$

These quantities are closely related to the device operating parameters. The value q_1 is also known as the gain of the device. The pixel (or microcell) recovery time, which measures the time from the onset of an avalanche to the moment when the diode is recharged to 95% of its full change, is equal to $3\tau_1$. The value of C_1 is roughly proportional to the area of the pixel, and varies by more than an order of magnitude between different devices, although for very small pixels a significant part of C_1 comes from the interconnects on the chip. Eq. 1 explains why, roughly speaking, SiPM's with high gain have fewer pixels per unit area than those with lower gain. Typical values for C_1 are in the range 15-150 fC. The value of R_q is also very important to understanding the behavior of the SiPM at high rates. Values vary from 100 kΩ to 100 MΩ, depending on the manufacturer.

The photon detection efficiency (PDE) is the product of the ratio of the active area to the total area of the chip, and the quantum efficiency ϵ of the APD's. The quantum efficiency is itself a product of several device and intrinsic properties, but tends to be in the range 50% - 70% around 500 nm for most devices, when operating at the optimum bias voltage. For the purpose of modeling the microscope readout, only the PDE is of any practical interest. It falls in the range 15%-25% at 490 nm, the peak wavelength for BCF-20 scintillator, for the devices considered in this study.

2.1 signal light yield

A Geant simulation of energy loss by a high-energy electron traveling through a 2 cm plastic scintillator fiber is shown by the yellow shaded region in the left panel of Fig. 1. The most-probable energy loss of 3.6 MeV agrees with expectations of roughly 1.8 MeV/cm in plastic. A fit to this spectrum with the Landau distribution was used to generate the signal pulse heights y_i for this study.

$$y_i = y_{mp}(1 + p\ell_i) \tag{3}$$

where the pseudo-random sequence ℓ_i is distributed according to the Landau distribution given in Eq. 4, and free parameters y_{mp}, p are displayed in Table 2.

$$f(\ell) = 12\pi i \int_{c-i\infty}^{c+i\infty} \exp(\ell s + s \ln s) ds \tag{4}$$

The pulse height distribution of signal pulses produced in the readout model simulation is shown for comparison in the right panel of Fig. 1. The horizontal axis is plotted in units of q_1 so that the effects of photon statistics are easy to estimate. The smearing out of the low-energy edge of the Landau peak in the right panel, as compared to the one in the left panel, is the result of the Poisson statistics in the discrete amplitude response of the SiPM.

The conversion factor from energy deposition to average photoelectron count (pixels firing) was obtained in the following way. Saint Gobain advertises that about 8000 photons are produced in

Table 2: Parameter values in the model pulse height density function Fig. 3. Values are dimensionless.

parameter	value
y_{mp}	200
p	0.17

the scintillation peak around 490 nm, per MeV of energy deposited by a minimum-ionizing particle. The capture fraction for the double-clad optical fiber is about 4.3% in each direction. With a 90% reflective coating on the upstream end of the fiber, a total of 650 photons per MeV are captured within the transmission aperture of the fiber. Assuming 33% losses the glue joint and along the length of the clear light guide, one expects a most-probable yield of 1600 green photons incident on the surface of the SiPM. A conservative PDE estimate of 15% leads to a most-probable pulse height of 230 pixels. This value has been rounded down to 200 pixels to produce the results reported below.

2.2 amplifier response

The response of the preamplifier and summing circuit to a single pixel firing has been modeled by a detailed impulse-response analysis of the circuit. The source is treated as a fast current spike with a total charge q_1 landing on input capacitance C_n and being drained off through the input impedance Z_i of the the amplifier. The parameter Z_i is a complex number that is frequency-dependent, but its value is on the order of 10 Ω. The preamplifier circuit was designed with a special input stage with low impedance in order to prevent the large capacitance C_n from producing long signal fall times $C_n\,|Z_i|$. The device capacitance C_n that appears in the expression for the single-pixel pulse width is *not* the C_1 that determines the gain factor according to Eq. 1, but includes the capacitance of all pixels in the device, plus the extra capacitance contained in the interconnection network on the chip. The value of C_n is in the range 150 - 300 pF for SiPM's that are large enough to read out a 2×2 mm fiber. The shape of the output voltage pulse driven into 50 Ω by the preamp in response to a single photoelectron is shown in Fig. 2. This shape is consistent with multi-photon pulses observed in bench tests with a fast-pulse laser diode, after unfolding with the diode pulse shape which was about 4 ns FWHM.

Note the long tail shown in the right panel of Fig. 2. The vertical scale has been expanded, relative to that in the left panel, to make the variation in the signal visible. It is extremely important to model the long tail correctly in the simulation because, at high rate, the tails from many pulses stack up on top of one another and produce a wandering baseline that underlies the fast component of following pulses. These baseline variations are equivalent to a meandering threshold in the discriminator, and limit the time resolution of the device at high rates. These effects are carefully modeled in this study.

2.3 pixel recovery

The primary purpose for the quench resistor is to isolate the diode from the bias voltage source, so that the junction potential drops below breakdown threshold as soon as a charge of q_1 has accumulated across the diode junction capacitance. To function in this way, the value of R_1 must be large enough to delay the recharging of the capacitance until all of the charges from the avalanche

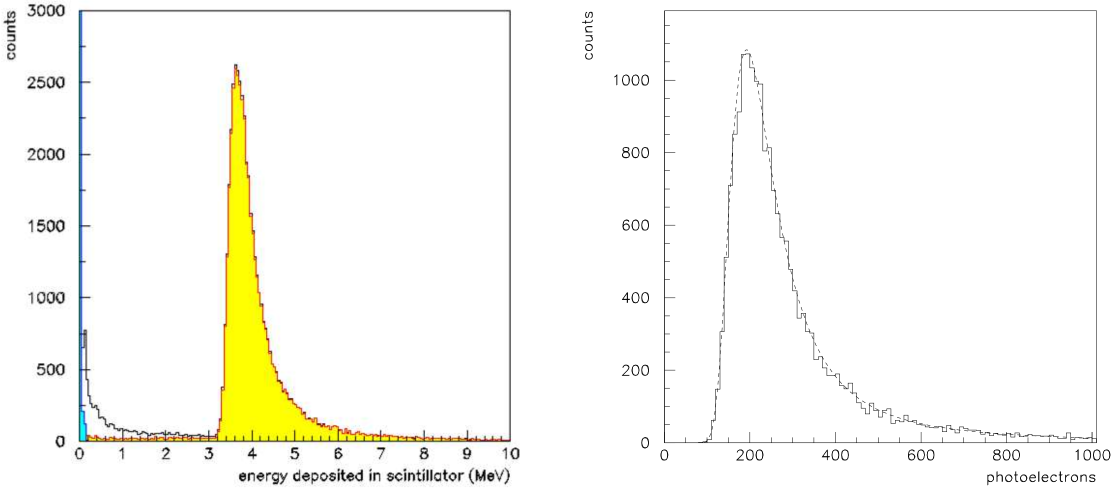

Figure 1: Energy deposition spectrum (left panel) and modeled photoelectron yield in a SiPM (right panel) for a 3 GeV post-bremsstrahlung electron in the Hall D tagger Geant simulation. In the left panel, the yellow shaded area corresponds to post-bremsstrahlung electron tracks, the blue peak near zero comes from gamma ray conversions in the plastic, and the black histogram is the complete spectrum, including the mostly low-energy hits from random room background. The spectrum in the right panel includes only the post-bremsstrahlung electron component, excluding the few percent below the Landau edge in the left plot that come from tracks entering or exiting the fiber from the side, that do not travel the full length inside the fiber. Cerenkov photons produced in the clear light guides fall outside the capture cone of the fiber, and are not included in the statistical model.

have been swept out of the depletion zone. For bulk of the charges, 100 ps would be sufficient delay to accomplish this [9], but a few of the charges inevitably get trapped in weakly bound localized states around defects. As soon as the junction potential is restored above breakdown threshold, a single one of these trapped charges can thermally excite out of its trap and induce a second avalanche.

This process known as “after-pulsing” is a property of all SiPM devices, although their effects are most noticeable in devices with small values of R_q like the ones from Hamamatsu. When these after-pulses were first observed in the Hamamatsu SiPM tested by our group, they were thought to be a defect of the device, but since then we have learned that they are the signature of a fast pixel recovery time, without which the device cannot function well at high rates. Provided that their probability remains significantly less than unity, after-pulses are a feature of fast SiPM devices, and simply add a long-tail component to the pulse shape for multi-photon pulses. As shown below, these after-pulses set the effective lower bound on the discriminator threshold that can be used in the microscope readout.

Several groups have published detailed measurements of the pixel recovery and after-pulsing behavior of SiPM’s from a variety of manufacturers [3–6]. Ref. [4] lists measured pixel recovery times for 14 different SiPM devices from 5 manufacturers, including CPTA and Hamamatsu. The value of 2.8 μs that they report for the CPTA 40×40 $\mu\mathrm{m}^2$ 556 pixel device is consistent with

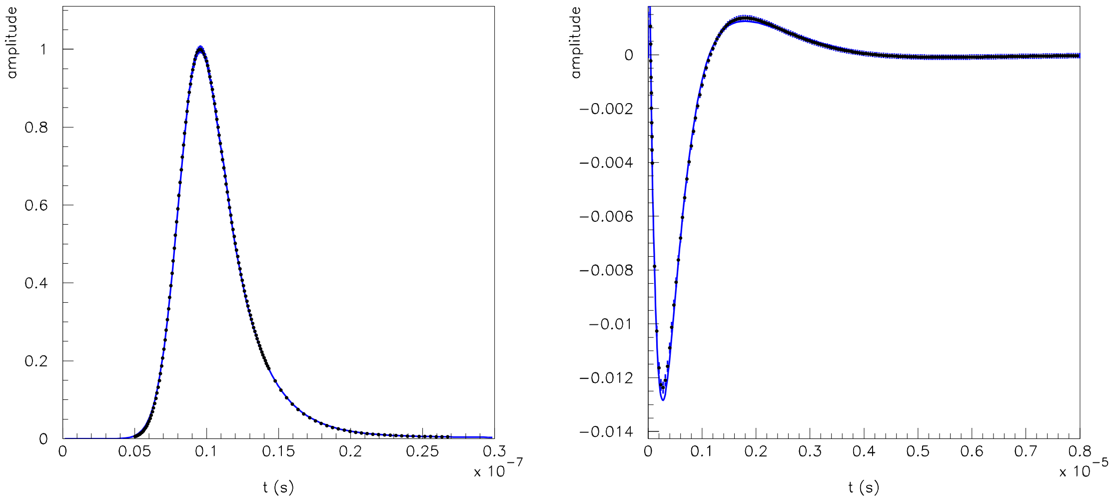

Figure 2: Detailed analytical model for a pulse from the UConn SiPM preamplifier circuit. The data points are computed from the Fourier transform coefficients of the circuit model, and the curve is a piece-wise analytic interpolation of the points. The second panel shows an expanded view of the tail of the pulse plotted in the first panel. The charge integral of the pulse is zero. The amplitude of the pulse is normalized to a maximum value of unity.

the large value of R_q of 7 MΩ reported in Ref. [3] for this device. Ref. [4] reports a wide range of recovery times for the 10 different Hamamatsu SiPM's they examined. Ref. [3] reports a R_q of 110 kΩ for the MPPC S10362-11-050C (400 50-micron pixels). Ref [7] reports a gain of 1×10^6 for this device at $\Delta V = 1$ V. Using Eqs. 1-2, these numbers give $\tau_1 = 16$ ns, and a 95% pixel recovery time of 48 ns for this device. Analyzing the data shown in Fig. 15 in Ref. [7] gives a more precise estimate of $\tau_1 = 10.9 \pm 1.4$ ns, which is more or less consistent with the value of 50 ns that is reported in Ref. [4] for the last two Hamamatsu devices listed in their Table 1.

Ref. [3] reports a much longer recovery time close to 200 ns for the S10362-11-050C. This may be due to the peculiar way that those authors used to measure the recovery time, by saturating the entire device with a 200,000 photon pulse and then following it after a variable delay with a smaller pulse whose amplitude is measured as a function of the delay. This method would induce additional recovery delays from whole-device effects, in addition to the single-pixel recovery times, so its disagreement with the manufacturer's reported value of 50 ns for the S10362 single-pixel recovery time is not surprising. Whole-device effects are probably less important for devices like the CPTA SiPM whose large value of R_q leads to single-pixel recovery times on the order of microseconds.

Hamamatsu markets its MPPC devices in three pixel sizes, for each choice of device size: 25, 50, and 100 microns. The gains of these devices vary by an order of magnitude, from 2×10^5 to 2×10^6. Eq. 2 implies that recovery times should scale with the gain, for fixed R_q. However slide 18 of Ref. [6] reports that Hamamatsu increases the value of R_q for devices with smaller pixels, which would offset this effect. This makes sense if the value of R_q was adapted by the manufacturer for each device, to keep the value of τ_1 constant, at the level needed to adequately suppress after-pulsing, while allowing for a maximum performance at high rates. Therefore a fixed value of $\tau_1 = 15$ ns was taken for the Hamamatsu SiPM simulated in this study, which is considered to be appropriate regardless of the actual pixel size chosen. Pixel recovery is modeled by assigning to each pixel that fires a time-dependent gain $g_1(t)$

$$g_1(t) = q_1(1 - e^{-t/\tau_1}) \tag{5}$$

where t is the time since that pixel last fired.

2.4 after-pulsing

The physical origin of after-pulse avalanches predicts that all pixels have independently random after-pulse events with exponential time distributions whose time constants are the lifetimes of the traps. Although in principle there may be many different time constants, one for each kind of traps, Ref. [5] reports that the observed after-pulse time distribution for MPPC devices can be adequately fit with just two time constants, one at 18 ns and the other around 70 ns. The probability integral for each of these after-pulse components depends steeply on the operating voltage ΔV. For this study, I assumed a value of $\Delta V = 1$ V, for which the two after-pulsing probabilities shown in Fig. 4 of Ref. [5] are 6% and 5%, respectively.

2.5 cross talk

The primary source of cross talk in a SiPM is an infrared photon produced in an avalanche in one pixel that is absorbed in a neighboring pixel and causes it to avalanche. Unlike after-pulses, cross-talk pulses occur essentially simultaneously with the avalanche that triggers them, and amounts to little more than a small increase in the overall gain of the device. Because they increase the observed pulse-height in multiples of the single-pixel response, they lead to larger widths than would be expected based on Poisson statistics. This effect does not impact the performance of the microscope in a significant way, but it is included in the simulation for completeness.

2.6 dark current

Dark current is caused by the random firing of pixels due to thermal excitations of charges creating spontaneous avalanches. Dark current I_d is related to dark rate per pixel r_1 through the following relation.

$$I_d = N q_1 r_1 \tag{6}$$

where N is the number of pixels in the device. The pixel dark rate r_1 generally scales with the volume of the depleted zone in the diode, varying from 300 Hz in the pristine MPPC S10931-025P to 9 kHz in the MPPC S10931-100P at room temperature and nominal operating bias [8].

The dark rates reported above have a negligible effect on the operation of the SiPM in the microscope readout. However, these numbers do not remain constant but increase over time as a result of exposure to elevated levels of ionizing radiation. Ref. [3] reports results from exposing SiPM's from a variety of manufacturers to 83 MeV protons. The principal effect seen in the SiPM's as a result of the exposure was an increase in the dark rate. They report the total radiation dose in their measurement as 2×10^10 /cm^2 of "1 MeV neutron equivalent flux". Using the conversion factor 1 rem = 2.4×10^7 n_{eq}/cm^2, this dose is equivalent to 830 rem. After irradiation, they observed a 30-fold increase in the dark rate for the Hamamatsu MPPC, and a similar factor for the CPTA/Photonique device. Ref. [1] reports a factor of 12 increase in dark current for the Hamamatsu MPPC after only 153 rem of neutron exposure. Comparison of these two results indicates that the slope of dark current vs. neutron dose is decreasing with increasing dose. This is also suggested by the slight negative curvature of the dark current vs. dose seen in the fourth plot in Ref. [1].

Operating the Hall D photon beam over a 10-year period (30,000 operating hours) at full beam intensity, an unshielded microscope readout would see a neutron dose of 5500 rem [2]. Surrounding the readout electronics with plastic shielding could easily reduce this number to 800 rem [2], which brings the dose into the range covered by Ref. [3], eliminating uncertainties from a large extrapolation. These estimates for dark rate increase vary from a factor 30, for a shielded readout solution, to a factor 400, for an unshielded readout and linear extrapolation based on Ref. [1]. In this study a number of scenarios are explored, with dark rates varying from a factor of 2 to 25,000.

3 Simulation Results

The parameter values used by the simulation model to produce the results reported below are given in Table 3. Note that the gain of the device is not included in the list. This is because all pulse heights are expressed in units of the single-pixel charge q_1. It is assumed that the preamplifier is capable of rescaling the output level to a range that is appropriate for the discriminator and ADC, and that the additional electronic noise from the preamplifier is negligible compared to the noise associated with after-pulsing and dark current when operating at rates appropriate for tagging. For reference, the prototype preamplifier built by the UConn group is designed to produce 2 mV peak output per photoelectron, for a most-probable expected output of 450 mV and an optimum discriminator threshold close to 100 mV. Judging by the ability to easily resolve individual photoelectron peaks in the SiPM pulse-height spectrum of the preamplifier output, the RMS electronic noise added by the preamp is smaller than 1 mV.

An important aspect of the simulation is its ability to take into account pile-up effects and the effects from AC couplings between various stages in the preamplifier, which create long oscillating tails on the back ends of the output pulses. The simulation started at t=0 with the state of the readout in quiescent condition and then ran forward for 3 μs, but only the last 1 μs was actually analyzed. This is what is meant by the parameters "length of trace simulated" and "length of trace analyzed" in Table 3.

The simulation consists of building up a trace of the output voltage on the preamplifier output in the following way. The elementary event in the simulation is the firing of a single pixel. Each time a pixel fires, a copy of the single-pixel output pulse shown in Fig. 2 is added with an appropriate time offset to the output trace. First dark-rate pulses are distributed randomly, one at a time, with the total number of them equal to the dark rate times the trace length. After that, signal pulses are generated with pulse heights distributed as illustrated in Fig. 1. Based on the generated pulse height, a Poisson random number of pixels are added to the trace, with their times starting at the t_0 of the pulse and distributed randomly according to the exponential decay with the time constant of the scintillator. After-pulses and cross-talk pulses are generated automatically each time a pixel event is produced. Each pixel generated modifies a full 2 μs of the output trace, because of the long oscillating tail that is present in the preamplifier response function. A sample trace is shown in Fig. 3. This trace was produced for the Hamamatsu MPPC with a signal rate of 4 MHz and a dark rate of 10 GHz. Both dark pulses and after-pulsing effects are visible, on top of the normal output pulse shape.

Once the trace is generated, it is analyzed to simulate the behavior of a leading-edge discriminator acting on the simulated signal. The analyzer steps through the trace watching for it to transition from below the threshold level to above. When this happens, the trace values below and above the threshold are interpolated to find the crossing time t_0. The value of the trace amplitude

Table 3: Parameters used by the simulation model to produce the results of this study. The CPTA device under study is the SSPM-0606BG4-PCB marketed by Photonique. The Hamamatsu device is the S10631-025P. Many of these parameters are not device-dependent and so are the same in both simulations.

parameter	CPTA SSPM	Hamamatsu MPPC
most-probable amplitude (photoelectrons)	200	200
scintillator time constant (ns)	2.7	2.7
discriminator threshold (photoelectrons)	50	50
discriminator minimum pulse separation (ns)	10	10
preamplifier impulse rise time (ns)	2.4	2.4
preamplifier impulse fall time (ns)	5.3	5.3
preamplifier peak delay time (ns)	9.5	9.5
preamplifier 50% delay time (ns)	7.8	7.8
mean tagged electron rate (MHz)	0.1-5	0.1-5
length of trace simulated (μs)	3	3
length of trace analyzed (μs)	1	1
size of time step simulated (ps)	100	100
dark rate for whole device (MHz)	$10\text{-}10^5$	$10\text{-}10^5$
total number of pixels in device	1700	14400
pixel recovery time constant (ns)	1000	15
cross-talk probability	0.13	0.02
short after-pulse time constant (ns)		18
short after-pulse probability		0.06
long after-pulse time constant (ns)		70
long after-pulse probability		0.05
number of traces generated per setting	20000	20000

a fixed time interval after t_0 is recorded as the pulse height for that pulse. For comparison with the generated value, the analyzer goes through the list of generated signal pulses and finds the one whose generated time plus a predefined offset is closest to the t_0 and matches up the generated time and amplitude with that found by the analyzer. The amplitude spectrum of the discriminated trace pulses analyzed in this way, divided by the generated spectrum, gives the detection efficiency of the readout as a function of pulse height. The ratio of the integrals of the two spectra gives the detection efficiency. It might be feared that measuring the efficiency this way might produce a bias on the high side, because spurious (noise) triggers are also counted, but the threshold used in this study was too high for this to occur at an appreciable rate. Its presence would be indicated by an extended flat background outside the peak in the time resolution plot, and this is not seen except at the highest dark rate 10^{11} Hz considered in this study.

3.1 results for the CPTA 2 mm device

To obtain baseline performance figures, the simulation was first carried out at a low signal rate of 100 kHz and a pristine dark rate for this device of 10^7 Hz. The generated and observed pulse height spectra are shown in the first panel of Fig. 4. The second panel shows the discriminator detection efficiency as a function of generated pulse amplitude. Fig. 5 shows the time-walk correction and

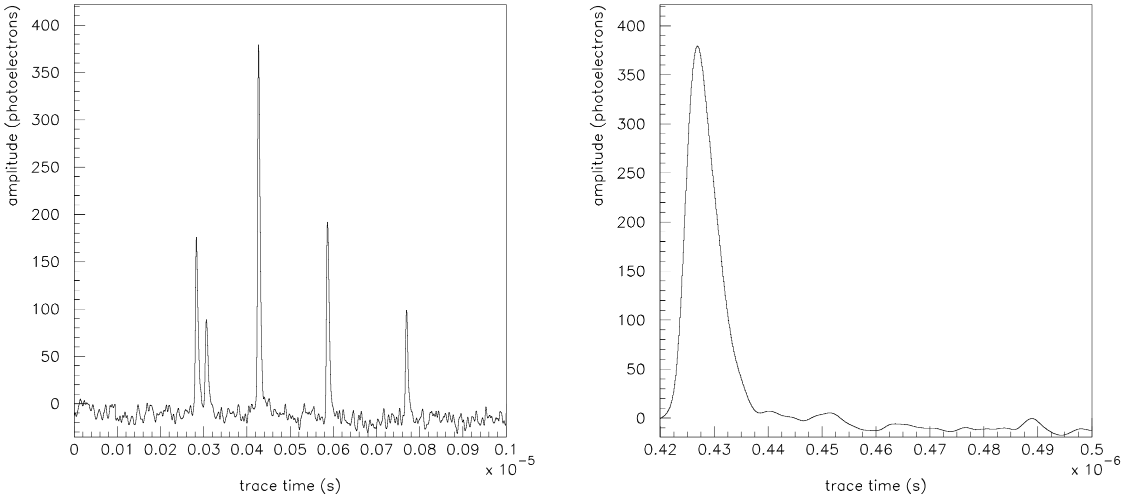

Figure 3: Sample trace taken from the simulation of the Hamamatsu MPPC at a signal rate of 4 MHz and a dark rate of 10 GHz. The y axis is output voltage expressed in units where a single pixel has a maximum amplitude of 1, as shown in Fig. 1. The second panel is a zoomed view of the first, showing the largest pulse in greater detail.

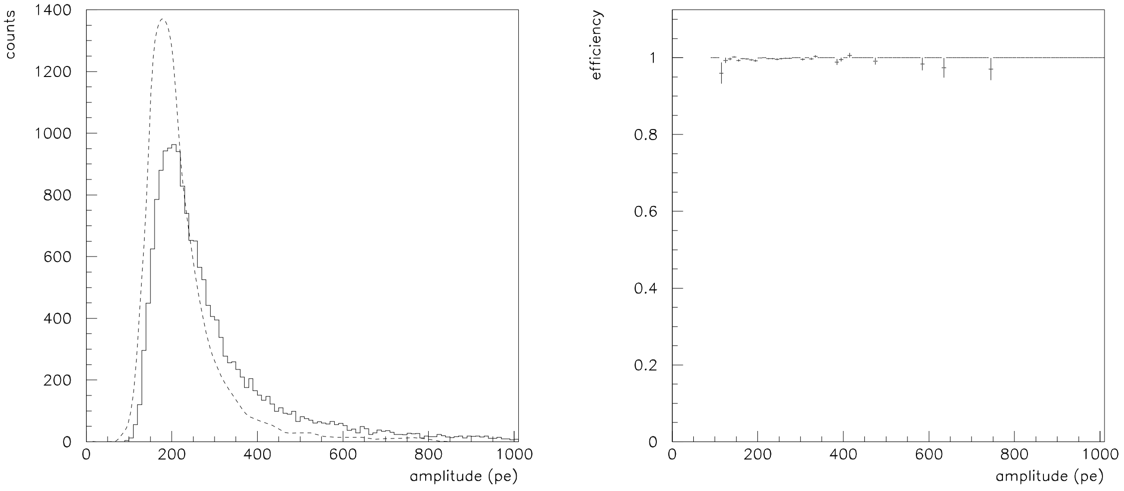

Figure 4: Amplitude spectrum (left panel) and detection efficiency as a function of amplitude (right panel) for the CPTA device simulation at a signal rate of 100 kHz and a dark rate of 10 MHz. The solid line in the left panel is the generated spectrum, and the dashed line is the spectrum of the detected pulses. The spectrum-weighted efficiency in this simulation is 99.8%.

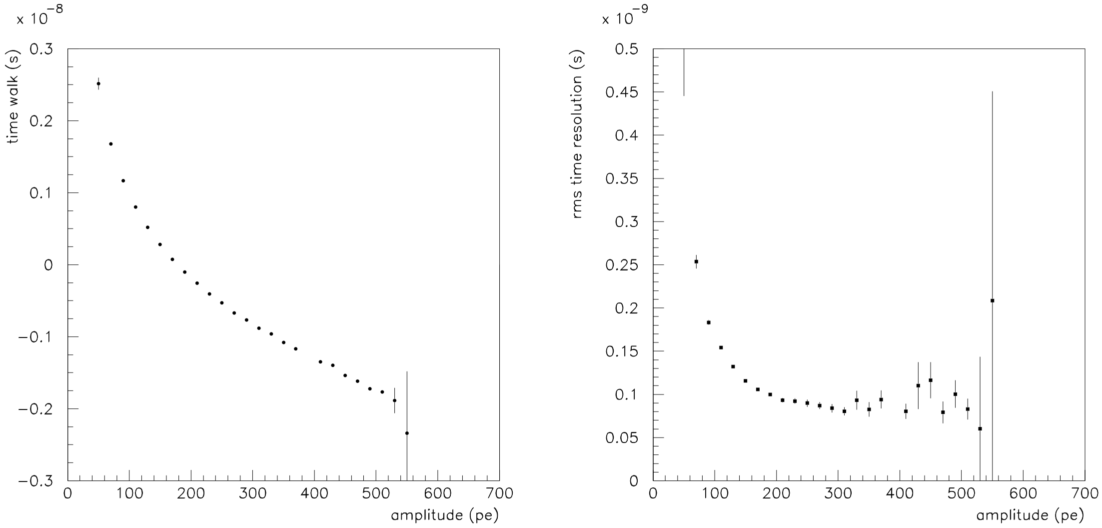

Figure 5: Time walk correction (left panel) and time resolution (right panel) as a function of pulse amplitude, for the CPTA device simulation at a signal rate of 100 kHz and a dark rate of 10 MHz. The spectrum-weighted RMS time resolution from this simulation is 122 ps.

RMS time resolution as a function of pulse amplitude under the same conditions. At 100 kHZ the CPTA device easily meets all of the performance requirements for the microscope readout.

Fig. 6 shows the generated and measured pulse amplitude spectra at signal rates of 1 MHz and 4 MHz. At the lower signal rate, there is a noticeable compression of the dynamic range coming from the limited number of 1700 pixels. This tends not to affect the time resolution very much because the missed photons tend to come from the tail of the pulse, whereas the leading edge is not affected. However at the operating rate of 4 MHz one starts to see a significant depression of the gain. This comes about in the simulation because of the high rate compared to the long pixel recovery time of 2.8 μs. The product of the rate and the average of 350 photoelectrons per pulse means that the average pixel firing rate is 800 kHz, with the result that the pixels rarely recover their full operating potential between firings. This might not be a problem if it were consistent, but the random nature of the events means that the effective gain is fluctuating from one signal pulse to the next by as much as a factor 2. Because of this, the pristine device detection efficiency drops from 98.5% to 92.5% between 1 MHz and 4 MHz counting rate.

These observations have nothing to do with elevated dark rate. The the simulations reported so far were run under pre-radiated conditions for the CPTA SSPM device. Things eventually get even worse when the dark rate is increased. The pristine dark rate is 6 KHz per pixel, small compared to the 800 kHz per pixel under operating conditions at 4 MHz. Dark rate begins to be noticeable as soon it becomes reaches the same magnitude as the signal rate per pixel, which occurs at about a factor of 100 times the pristine rate, or 10^9 Hz. Fig. 7 compares the time resolutions at 4 MHz signal rate between device dark rates of 10^7 Hz and 10^9 Hz. The time resolution has degraded somewhat with increasing dark rate, but the most important effect is on the detection efficiency. At 4 MHz signal rate and 10^9 Hz dark rate, the detection efficiency at the discriminator threshold of 50 pe has dropped to only 56%.

In summary, the pre-radiated CPTA device marginally satisfies the efficiency specification of

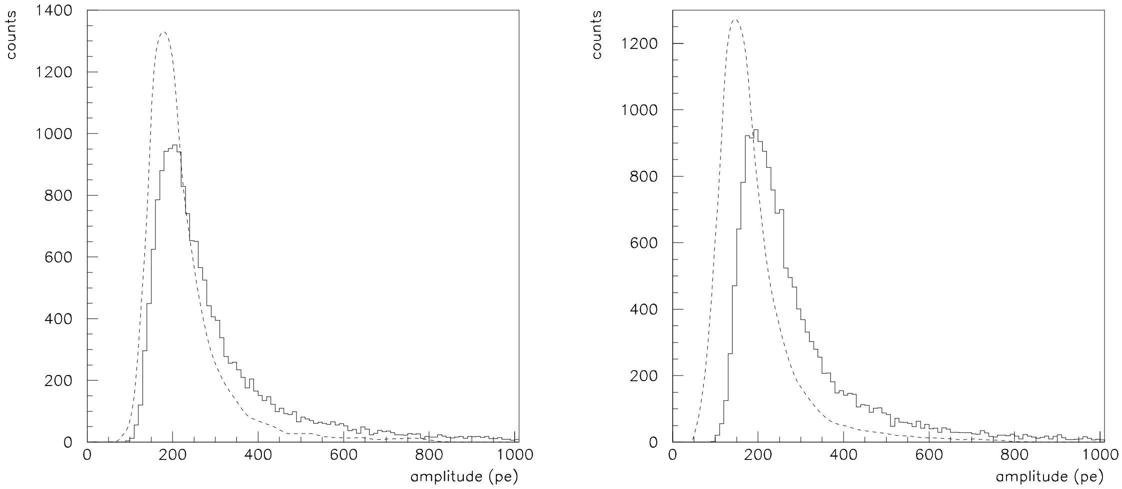

Figure 6: Pulse height amplitude spectrum for the CPTA simulation at a signal rate of 1 MHz (left panel) and 4 MHz (right panel). The solid lines are the generated amplitude spectra and the dashed lines are the detected pulse heights. The spectrum-weighted detection efficiencies are 98.5% and 92.5%, respectively.

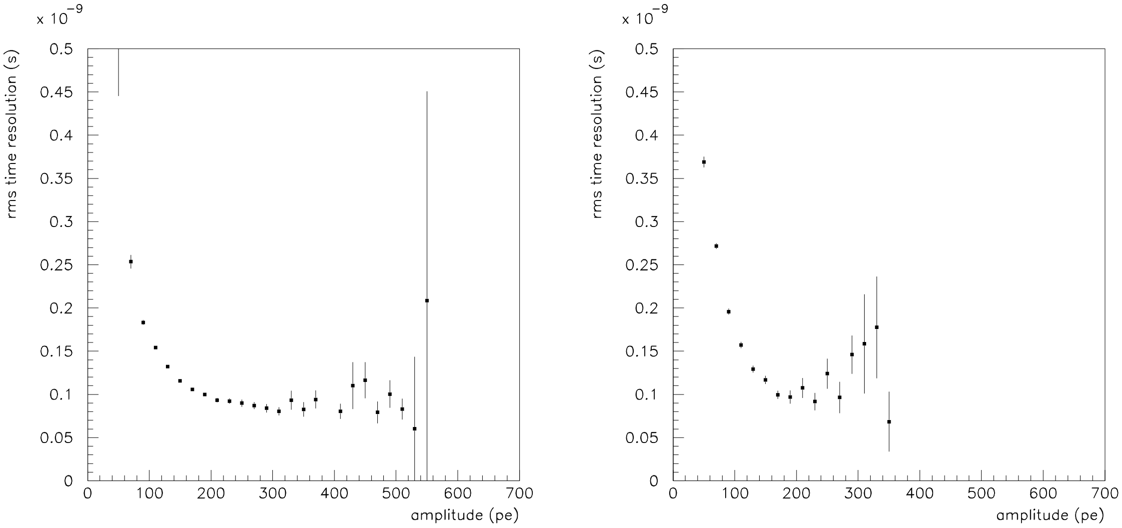

Figure 7: RMS time resolution for the CPTA device at a signal rate of 4 MHz and dark rate of 10 MHz (left panel) and 1 GHz (right panel). The corresponding spectrum-averaged resolutions are 176 ps and 228 ps, respectively. The discriminator detection efficiencies at 50 pe threshold are 92.5% and 55.3%, respectively.

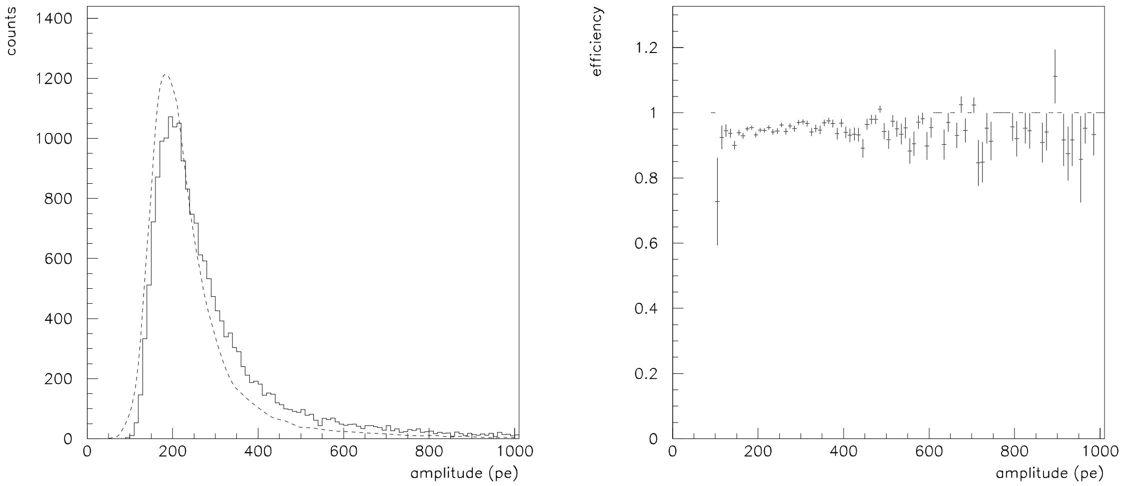

Figure 8: Amplitude spectrum (left panel) and detection efficiency as a function of amplitude (right panel) for the Hamamatsu device simulation at a signal rate of 4 MHz and a dark rate of 10 MHz. The solid line in the left panel is the generated spectrum, and the dashed line is the spectrum of the detected pulses. The spectrum-weighted efficiency in this simulation is 94.8%.

95% at the full operating rate of a microscope channel, which is somewhat under 4 MHz, but it is already operating at a current higher than is optimum for this device, because of its long pixel recovery time. If radiation damage causes the dark rate to increase by a factor 100 above that of the pristine device, the gain fluctuations caused by the long pixel recovery time seriously impact the efficiency of the detector, to the point where it cannot function adequately for the purposes of tagging. One could recover most of the lost efficiency by reducing the discriminator threshold to 20 pe, or perhaps even to 10 pe, but at some level it begins to see a substantial rate of false hits from dark current pile-up. Further optimization of the simulation based on the CPTA device was not attempted because running this device above 1 MHz seems already to be stretching its capabilities, even in the absence of elevated dark current. Beside that, it would seem to be a waste of time to squeeze the last ounce of performance out of the Photonique SSPM, when one compares it to the Hamamatsu MPPC device treated in the next section.

3.2 results for the Hamamatsu 3 mm device

Fig. 8 shows the amplitude spectrum, and the detection efficiency as a function of generated amplitude, for the pristine MPPC device running at 4 MHz. The Hamamatsu MPPC considered in this simulation has a considerably smaller geometric fill factor than the CPTA SSPM device (25 micron vs. 50 micron pixels), but its intrinsic quantum efficiency peaks in the green-blue region, whereas the CPTA device QE peaks in the red. The net effect is that the two devices have similar PDE values for light from BCF-20 scintillator, here taken to be 15%. This is why the generated pulse height distribution comes out to be the same in the two simulations, as can be seen by comparing the solid histograms in Figs 6 and 8, left panel. The measured pulse height distributions are different, however, because the non-linearity and pixel-recovery effects are different in the two cases. Note that the large number of pixels and the fast pixel recovery time make the measured

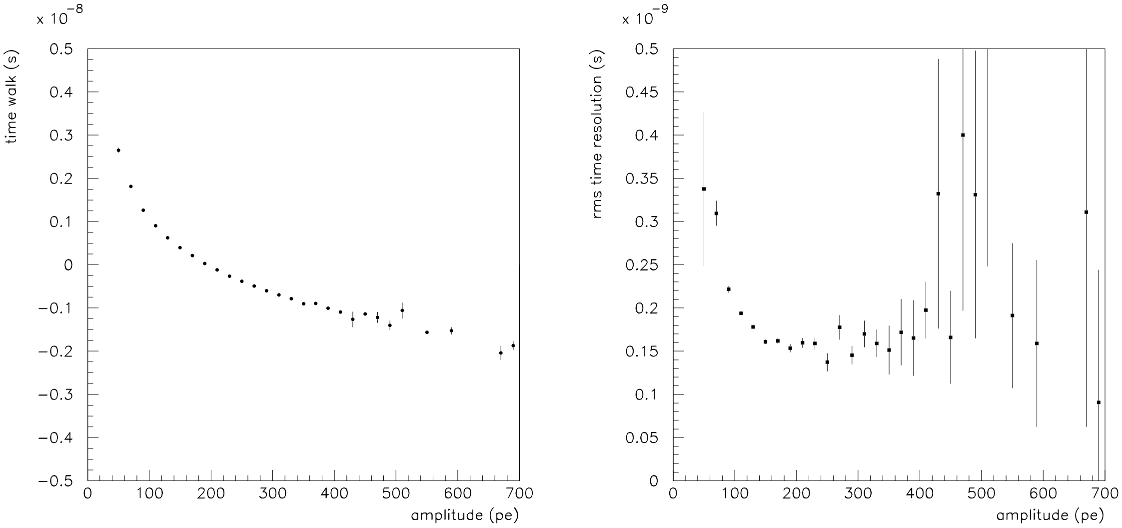

Figure 9: Time walk correction (left panel) and time resolution (right panel) as a function of pulse amplitude, for the MPPC device simulation at a signal rate of 4 MHz and a dark rate of 10 MHz. The spectrum-weighted RMS time resolution from this simulation is 181 ps.

spectrum much closer to the generated one in the case of the MPPC device than was seen for the SSPM, but in both cases some amount of dynamic range compression is visible in the suppression of the Landau tail.

The time walk correction and RMS time resolution functions are shown in Fig. 9 for the pristine MPPC running at the maximum expected operating signal rate of 4 MHz. Comparison with Fig. 8 shows that the time resolution in the region of the peak amplitude is better than 200 ps, satisfying the design goal for RMS time resolution under running conditions.

To track how these performance parameters degrade with increasing dark rate, the plots in Figs. 8-9 were repeated at device dark rates of 100 MHz, 1 GHz, 10 GHz, and 100 GHz. Dark rate effects were not noticeable at 100 MHz and 1 GHz, but they become significant at 10 GHz, and at 100 GHz the performance of the device is badly impaired. Fig. 10 shows the generated and measured amplitude spectra for the highest two dark rates simulated. In all of these dark rate studies, the signal rate was kept constant at 4 MHz so that all differences from what was shown in Figs. 8-9 would be due to dark rate effects alone. Visual comparison of these spectra suggest that the readout is still functioning at 10 GHz dark rate essentially as it did when it was new at 4 MHz, but at 100 GHz it is showing substantial pe yield fluctuations. The corresponding RMS time resolutions and detection efficiencies are shown in Figs. 11-12.

These results are summarized in Table 4 for the full range of dark rates studied. Considered together, they show that the readout is able to function at an acceptable level at a dark rate up to as high as 10 GHz, but not much higher.

4 Conclusions

Operating the Hall D photon beam over a 10-year period (30,000 operating hours) at full beam intensity, an unshielded microscope readout would see a neutron dose of 5500 rem [2]. Surrounding

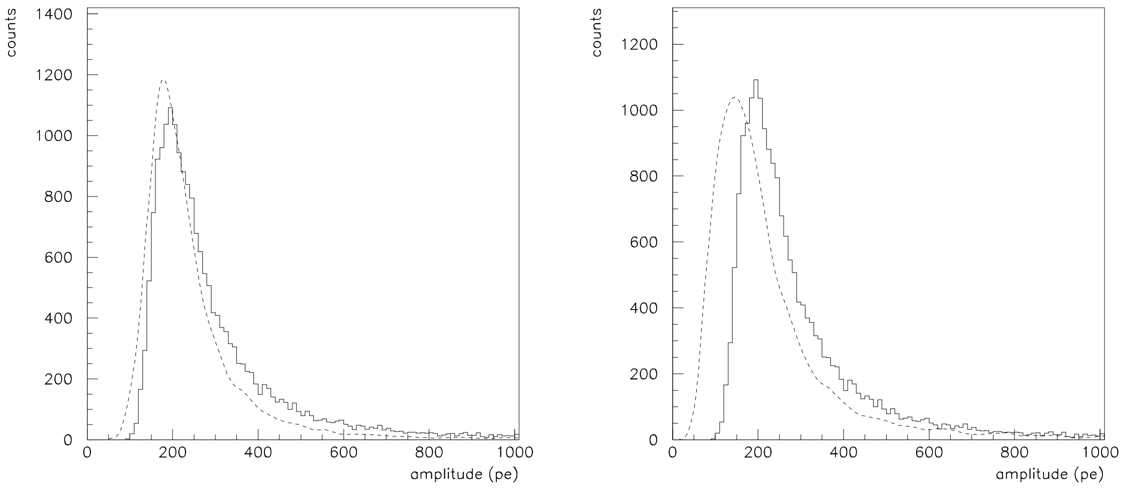

Figure 10: Amplitude spectra for the MPPC device operating at a signal rate of 4 MHz with a whole-device dark rate of 10 GHz (left panel) and 100 GHz (right panel). The solid line is the generated spectrum, and the dashed line is the spectrum of the detected pulses.

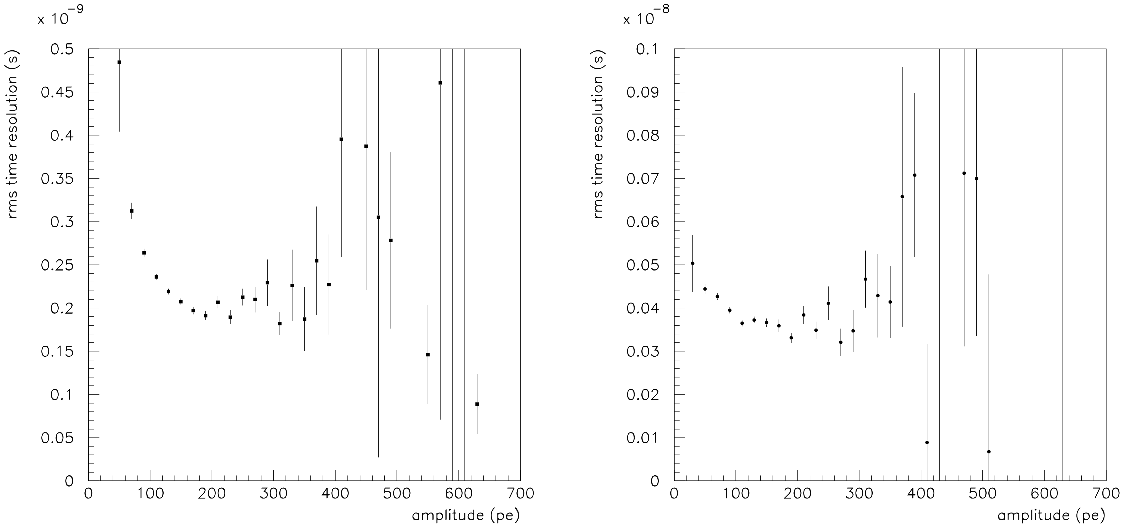

Figure 11: RMS time resolution as a function of pulse amplitude for the MPPC device operating at a signal rate of 4 MHz with a whole-device dark rate of 10 GHz (left panel) and 100 GHz (right panel). The discriminator threshold was left fixed at 50 pe.

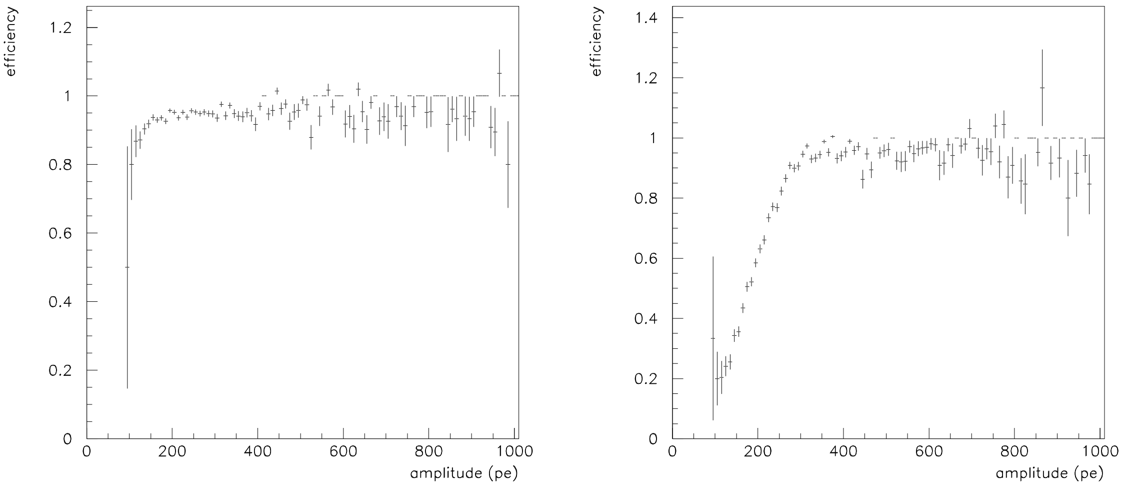

Figure 12: Detection efficiency as a function of generated amplitude for the MPPC device operating at a signal rate of 4 MHz and a dark rate of 10 GHz (left panel) and 100 GHz (right panel). The discriminator threshold was left fixed at 50 pe.

Table 4: Time resolution and detection efficiency for different levels of dark rate. Dark rates stated are whole-device counts per second.

device	signal	dark rate		time resolution		efficiency	
SSPM	4 MHz	10	MHz	166	ps	92.5	%
		100	MHz	167	ps	91.7	%
		1	GHz	195	ps	55.3	%
		10	GHz	-		0.0	%
MPPC	4 MHz	10	MHz	181	ps	94.8	%
		100	MHz	183	ps	94.9	%
		1	GHz	188	ps	94.9	%
		10	GHz	225	ps	94.7	%
		100	GHz	381	ps	73.8	%

the readout electronics with plastic shielding could easily reduce this number to 800 rem [2], which brings the dose into the range covered by Ref. [3], eliminating uncertainties from a large extrapolation. Linear extrapolation of dark rate increase from 150 rem to 5500 rem, based on Ref. [1], predicts a growth in dark rate by the factor 440 for the Hamamatsu MPPC device. Linear extrapolation of the dark rate increase from 830 rem to 5500 rem, based on Ref. [3], predicts a growth in dark rate by the factor 200. The smaller value is consistent with the slower-than-linear growth of dark rate with radiation dose shown in Ref. [1]. For the Hamamatsu S10931-025P MPPC, these predictions lead to dark rates of 1.8×10^9 Hz and 8×10^8 Hz, respectively, at the end of the 10-year period. Both of these rates are far less than the upper bound of 10 GHz for the dark rate, based on this simulation study.

These estimates do reply on extrapolations well beyond the range of existing radiation damage measurements. Evidence up to 800 rem points to less-than-linear dark rate growth with radiation dose, but there is some risk entailed in assuming that this trend continues up to 5500 rem. Somov has shown [2] that a relatively simple shielding scenario, employing sheets of plastic as neutron moderators around the readout, can reduce the neutron dose seen by the MPPC devices by a factor of 6. Doing this would bring the projected dose over a 10-year period down to the same level as reported in Ref. [3], thus avoiding extrapolation uncertainties.

Based on this study, the impact of radiation damage on the performance of the tagger microscope readout based on Hamamatsu MPPC devices is expected to be negligible over the projected lifetime of the detector. Shielding the readout with sheets of plastic to moderate fast neutrons is recommended to control risks associated with extrapolation of existing radiation damage measurements. It would also be useful to extend the range of existing radiation damage measurements on these devices up to the level of 5000 rem, to test the validity of the extrapolation model for the dark rate, and also to check if other effects on the operating characteristics begin to emerge at these higher levels of radiation damage.

References

[1] Y. Qiang, "SiPM Radiation Hardness Test", report available at `http://www.jlab.org/Hall-D/software/wiki/index.php/SiPM_Radiation_Hardness_Test`

[2] A. Somov, "Neutron Background Estimates in the Tagger Hall", *gluex-doc-1646*, 2010.

[3] Y. Musienko, D. Renker, Z. Charifoulline, K. Deiters, S. Reucroft, and J. Swain, "Study of Radiation Damage Induced by 82 MeV Protons on Multi-pixel Geiger-Mode Avalanche Photodiodes", Nucl. Instr. Meth. **A610** (2009) 87-92.

[4] I. Britvitcha, and D. Renker, "Measurements of the Recovery Time of Geiger-Mode Avalanche Photodiodes", Nucl. Instr. Meth. **A567** (2006) 260-263.

[5] F. Retière, "MPPC Response Simulation and High Speed Readout Optimization", Nuclear Science Symposium Conference Record (NSS/MIC), 2009 IEEE Issue Oct. 24 2009-Nov. 1 2009, 2197-2200.

[6] A. Para, "First Look at the Hamamatsu MPPC", FNAL Research Techniques Seminar, Nov. 8, 2007, slides available online at `http://www-ppd.fnal.gov/EPPOffice-W/Research_Techniques_Seminar/Talks/Para_SiPM_RTS_1.ppt`

[7] "Technical Information: MPPC Multi-Pixel Photon Counter", Solid State Division, Hamamatsu, available online at `http://sales.hamamatsu.com/assets/applications/SSD/mppc_kapd9003e02.pdf`.

[8] "MPPC Multi-Pixel Photon Counter S10362-33/S10931 Series", Solid State Division, Hamamatsu, available online at `http://jp.hamamatsu.com/resources/products/ssd/pdf/s10362-33series_kapd1023e05.pdf`.

[9] R. Vinke, H. Löhner, D.R. Schaart, H.T. vanDam, S. Seifert, F.J. Beekman, and P. Dendooven, "Optimizing the Timing Resolution for use in TOF-PET Detectors", Nucl. Instr. Meth. **A610** (2009) 188-191.

[10] S. Seifert, H.T. vanDam, J. Huizenga, R. Vinke, P. Dendooven, H. Löhner, and D.R. Schaart, "Simulation of Silicon Photomultiplier Signals", IEEE Transactions on Nuclear Science, vol. 56, no. 6 (2009) 3726-3733.

[11] R. Vinke, H. Löhner, D.R. Schaart, H.T. vanDam, S. Seifert, F.J. Beekman, and P. Dendooven, "Time Walk Correction for TOF-PET Detectors based on a Monolithic Scintillation Crystal Coupled to a Photosensor Array", Nucl. Instr. Meth. **A621** (2010) 595-604.